Green Synthesis and Characterization of Moringa Extract Fe-TiO₂ Nanocomposites for Efficient Photodegradation of Methylene Blue from Wastewater

[1]Ayesha Noor, [1]Muhammad Irfan*, [1]Alishba Qureshi, [1]Somia Bibi, [2]M. Naziruddin Khan,
[3]Fatimah M. Alzahrani, [4]Wissem Mnif

[1]Department of Physics, Government Girls Degree College No 2 D I Khan, 29111, KPK, Pakistan.
[2]Department of Physics, Faculty of Science, Islamic University of Madinah, Madinah, 42351, Saudi Arabia
[3]Department of Chemistry, College of Science, Princess Nourah bint Abdulrahman University, P.O. Box 84427, Riyadh 11671, Saudi Arabia
[4]Department of Chemistry, Faculty of Sciences at Bisha, University of Bisha, P.O. BOX 199, Bisha 61922, Saudi Arabia
m.irfan6570@gmail.com*

Summary: In this study, iron-doped titanium dioxide (TiO₂) nanocomposites were synthesized using *Moringa oleifera* leaf extract via a green two-step sol-gel method, aiming to enhance photocatalytic degradation performance under sunlight. The *Moringa*-mediated synthesis provided an eco-friendly and cost-effective route for obtaining Fe-doped TiO₂ nanomaterials (MFTNc) with improved structural and optical characteristics. X-ray diffraction (XRD) confirmed the anatase phase and revealed a reduction in crystallite size with increasing Fe content, while FTIR analysis validated the presence of key functional groups and Fe–O–Ti bonding. UV–Vis spectroscopy demonstrated a significant redshift in absorption and narrowing of the band gap from 3.21 eV (pure TiO₂) to 2.98 eV (0.9% Fe-doped TiO₂), enabling visible light activation. The photocatalytic activity was evaluated through the degradation of methylene blue (MB) under solar irradiation. The 0.9% Fe-doped TiO₂ sample exhibited the highest degradation efficiency (22.5%), significantly outperforming pure TiO₂ (9.25%) due to enhanced charge carrier separation and reactive oxygen species (ROS) generation. These results highlight the potential of MFTNc as a sustainable and efficient photocatalyst for environmental remediation applications.

Keywords: Fe-doped TiO₂ nanocomposites MFTNc; Efficient Photodegradation of MB; Wastewater Treatments; Photocatalysis; Crystal Structure.

Introduction

Water contamination has risen in the modern era as a result of population development and industrialization. Water contamination is one of the most pressing environmental challenges worldwide [1, 2]. Water contamination has risen in the modern era as a result of population development, and in contemporary times, artificial boards or color materials generate significant amounts of reducing organic compounds (ROCs), which have the potential to harm indoor air quality [3-5]. One of the most prevalent methods to eliminate ROCs from indoor air environments, among the latest technological developments, is the photocatalytic degradation of ROCs. To provide color to commercial items, dyes are widely employed in the production of fabrics, leather, color printing, food flavors, plastic, and cosmetics. However, low concentrations of dyes in industrial wastewater are very visible and undesired [6], [7], [8], [9]. The release of various toxic dyes from major textile manufacturers into wastewater is a major factor in serious environmental problems [10]. They have mutagenic and carcinogenic qualities and can harm the

aquatic ecosystem and human health, including renal, reproductive, liver, brain, and central nervous system disorders [6]. An estimated 1–20 % of the dye used in the textile industry disappears during processing and ends up in the environment [11]. The issue of water contamination has become a significant concern as the population and textile manufacturing have risen [12]. Numerous methods, including mineral precipitation and retention on the broad surface area, are used to remove these harmful pigments from water [13], biological membranes [14], and ion-exchange processes [10], flocculation, carbon adsorption [15], reverse osmosis, activated sludge process, and biological methods [16]. Using the photo-induced process is one of the possible remedies [12]. The significance of photocatalysts in our daily lives is their low cost, non-toxicity, and chemical/thermal stability [17]. Heterogeneous semiconductor photocatalysis is recognized as an effective way of degrading organic contaminants in water and addressing the worldwide energy shortage [18]. It is generally understood that morphological and structural characteristics have a

---

*To whom all correspondence should be addressed.

significant impact on a semiconductor's photocatalytic activity [19]. The semiconductor produces highly oxidizing free radicals upon photon exposure, enabling the degradation of materials adsorbed on its surface [20]. Among the several large band gap metal oxide semiconductors, such as NiO, ZnO, WO_3, SiC, TiO_2, CuO, and Nb_2O_5 [21]. Among all the researched metal-oxide nanostructures, TiO_2 has been widely employed [18], and Numerous studies have focused on the synthesis and modification of titanium dioxide, one of the most significant photocatalysts [22]. Since (TiO_2) is non-toxic, inexpensive, and has a reasonably high efficacy, it is frequently utilized as a photocatalyst in chemical and biological stability [23]. However, two disadvantages limit the application of TiO_2: Fast recombination of Photogenerated charge carriers; a large band gap, which is approximately 3.0 eV for the rutile phase and 3.2 eV for the anatase phase, which limits absorption of light in the visible range. As a result, pristine TiO_2 acts as an active photodegradation material in the UV light region (only 4-5% present in solar radiation) compared to the visible light spectrum [20]. Whereas rutile TiO_2 absorbs in the visible area (410 nm), it has lower photocatalytic activity compared to the anatase phase, which is triggered by ultraviolet light in the wavelength (385 nm) [19]. The primary goal of iron doping is to activate TiO_2 under visible light and improve its photocatalytic performance [24]. A dopant ion can function as an electron trap, enhancing the photocatalytic activity of TiO_2 by reducing the recombination rate of electron-hole pairs [16]. The impact of doping on activity varies depending on parameters such as method, type, and concentration of dopant [22]. Several investigations have concentrated on developing visible-responsive TiO_2 photocatalysts through loading with Nobel-metal, non-metal ions or forming heterojunctions with other semiconductors [25]. Transition metal-doped TiO_2 has been used extensively to enhance both the interaction with the visible portion of the light spectrum and the photo performance of the electronic methods [22]. Loading TiO_2 with transition-metal ions has been observed to influence its properties significantly, such as Fe [26], Co [27], Mn [28], and Ni ions [29], effectively increases its photocatalytic activity [25]. The Fe^{3+} ion among transition metal ions, it has garnered significant interest because of its half-filled d-electronic conFiguration and the same ionic radii between Fe (0.64Å) and Ti (0.68 Å), indicating that it may incorporate into the composition of the TiO_2 lattice [18][30]. Several investigations showed that introducing Fe to modified TiO_2 could significantly increase its photocatalytic activity [31][6], [26], [32]. In this study Moringa plant extract is utilized for, Fe loading into TiO_2 matrix was employed to enhance the photocatalytic activity of TiO_2. Bioactive substances such as flavonoids, phenolics, and ascorbic acid, which are abundant in moringa plant extract, serve as potent stabilizing and reducing agents in green synthesis. Effective nanoparticle formation with regulated size and stability is facilitated by these phytochemicals. Moringa has a higher antioxidant content than other plants, which improves the synthetic material's functional performance [33], [34]. Fe^{3+} ions behave as electron-hole traps, increasing the lifespan of electron-holes and hence enhancing the photocatalytic activity of TiO_2 [35]. It is thought that the addition of Fe^{3+} ions to the TiO_2 lattice weakens the banding of nearby oxygen atoms, allowing oxygen atoms to be easily released from the lattice and creating an oxygen vacancy. This allows for the adsorption of more oxygen, H_2O, and hydrogen ions onto the surface of TiO_2 catalysts, which lowers the conduction band electrons and increases the photocatalytic activity of Fe-doped TiO_2 [36]. Many techniques have been used to create undoped and doped TiO_2 nanoparticles in a variety of sizes and morphologies, including chemical vapor deposition, traditional sputter-deposition technique, and various hydrothermal processes. However, these approaches necessitated specialized equipment, complex control systems, high temperatures, and vacuums, all of which were costly. As a result, it is essential to identify a low-cost solution. In recent years, the sol-gel method was introduced as a flexible way to create the Fe doped TiO_2 nanostructure since it is cost-effective, simple to use, and does not require harsh experimental conditions [31].

This study represents the synthesis of Fe-doped TiO_2 nanocomposites using Moringa leaf extract (MFTNc) through a green sol-gel method. The unique role of Moringa leaf extract as a natural stabilizing and inhibiting ingredient not only ensures an eco-friendly synthesis route but also enhances the structural, physio-optical, and photocatalytic characteristics of the resulting MFTNc. Improved photocatalytic performance, superior optical absorption, and reduced recombination rate of electrons and holes might be due to the production of highly crystalline material via a simple, eco-friendly, and economical two-step sol-gel synthesis approach. Improved optical and photocatalytic properties make MFTNc a more suitable candidate for sustainable wastewater treatments.

Experimental

Materials and Methods

The undoped and MFTNc nanocomposites were prepared employing a two-step

sol-gel approach. All of the preliminary substances, including titanium butoxide (IV) Ti (OBu)$_4$, iron nitrate nonahydrate Fe (NO$_3$)$_3$•9H$_2$O, acid as a stimulant (HCl), and deionized water (DI), were acquired from Sigma Aldrich (Germany) and ANALAR.

Synthesis of Moringa Leaf Extract

10 g of fresh Moringa leaf was taken and washed several times with distilled water, and then placed in a dry oven for dehydration at 80 $^{\circ}$C. The dried leaves of Moringa were ground into fine powder, and after 30 minutes of boiling in 50 mL of water, the solution was obtained to obtain pure Moringa extract was obtained. Placed in a refrigerator at 4 ^{0}C for further use.

Preparation of MFTNc

A mixture of 20 ml of purified water and 10 ml of titanium butoxide (TBO) has been utilized as the precursor ingredients. The solution was stirred continuously for 20 minutes at room temperature (60 $^{\circ}$C). During continuous stirring, 0.7g powder of Fe (NO$_3$)$_3$•9H$_2$O (0.05 mol / L) was mixed in the solution along with 5 mL of Moringa extract as a stabilizing and reducing agent was added dropwise, and the stirring was stopped after the next 40 min. To create xerogel, the heated specimens were then dried for six hours at 150 $^{\circ}$C in a heated oven. After that, broad crystals developed, signifying that the gel had completely dried. The dried gel is crushed and pestled into fine powder. The specimen was calcined for four hours at 400 °C for the removal of any potential impurities that break down at this temperature. The same procedure was adopted for 0.9 % Fe-doped samples, and additionally, (0.9 g) of Iron nitrate non-hydrate Fe (NO$_3$)$_3$•9H$_2$O (0.06 mol / L) was mixed in the solution.

Photocatalytic Activity

Methylene blue (MB) was used as a starting dye concentration of 10 mg per 500 milliliters for 0.5 mg of Fe-doped TiO$_2$ nanocatalysts for every 100 milliliters of MB solutions to measure the rate of degradation after the produced MFTNc were exposed to natural sunlight. Each specimen was exposed to various intervals of direct sunlight to analyze its UV-vis absorption spectra and determine its photocatalytic capacity. In Lahore, Pakistan, where the sunshine intensity was much lower (1.5 W m^{-2} s^{-1}), the available sunshine exposure duration varied from 0 to 80 minutes, with a 10-minute break in March. Specimens of the MB solution were then taken and examined using UV-visible spectroscopy at λ max = 470 nm after being exposed to direct sunlight for 10 minutes. The photocatalytic ability of MFTNc that induces MB decomposition was determined using the formula given in Equation 1:

$$\text{Degradation Efficiency (\%)} = \frac{c_t - c_0}{c_o} \, 100 \ \% \quad (1)$$

Results and Discussions

XRD

The XRD approach is commonly used to examine the crystalline arrangement and phase composition of various semiconductors. The XRD structure in Fig 1 indicates that for TiO$_2$ all of the diffraction peaks anatase observed at 2 theta brags angles of 25, 38, 48, 55, and 62^0 corresponded to the (1 0 1), (1 1 2), (2 0 0), (2 1 1) and (2 1 5) planes respectively with lacking of rutile peaks [37], [38]. In light of the XRD graph of the MFTNc specimens, the BCC face Fe (JCPDSN$_0$-0089-4921) diffraction peaks, (except that of pure TiO$_2$), which were detected at 2θ values of 37, 63 respectively, were indexed to the (0 0 4), (2 1 5) planes [37], [38]. Consequently, the XRD investigations demonstrated that only the anatase phase is present across both TiO$_2$ and MFTNc [37]. The intensity of a sample's diffraction peaks has been observed to affect its crystallinity. The undoped TiO$_2$ photocatalyst had the maximum peak intensity, which reduced with the rise in the Fe doping concentration in the TiO$_2$ crystal. XRD results suggest that the TiO$_2$ nano composites' crystallinity was varied significantly by the incorporation of Fe^{3+} ions [39]. Fe^{3+} ions probably help nucleation and crystal growth in the TiO$_2$ matrix, which explains the initial increase in crystallinity at 0.7% Fe doping. Excess Fe, however, causes lattice strain and defects above this ideal concentration (0.9%), which breaks the crystal structure and lowers crystallinity. This trade-off shows that while excessive doping causes structural disorder, moderate doping can improve order. To balance enhanced crystallinity and prevent degradation brought on by defects, dopant concentration optimization is essential. The anatase diffraction peaks were used to estimate the crystallite sizes using the Scherrer equation.

$$D = k\lambda / \beta \text{Cos}\theta \quad \text{(i)}$$

In the above Scherrer relation, λ represents the wavelength of incident X-rays, β shows the entire width at half maximum (FWHM) corresponding to the scattering peak, D indicates the average crystallite size, and k is a value that remains

constant (0.94) [37]. The average crystallite size of the TiO₂ nanocrystal reduces significantly with gradual increases in Fe content from (0.7 to 0.9) %. Our XRD statistics, as shown in Table I, fully satisfy the Scherer formula, which states that crystallite size declines with peak broadness (FWHM) and that the size of crystalline particles (D) is inversely related to peak stretching. Fe doping introduces lattice strain and defects into the TiO₂ crystal structure, which causes peak broadening in XRD. When Fe^{3+} replaces Ti^{4+} in the lattice, local distortions are produced due to the smaller ionic radius of Fe^{3+} (0.64 Å) than Ti^{4+} (0.68 Å). These distortions cause micro-strain and interfere with long-range crystallinity. Fe incorporation also prevents crystal growth, which leads to smaller crystallite sizes and, according to the Scherrer equation, broader peaks. Diffraction coherence is also impacted by the increased disorder. Therefore, when Fe is doped, the XRD peaks are widened by the combined effects of strain and size. As the concentration of Fe increases from (0.7 to 0.9) %, the average crystallite size of the pure TiO₂ crystallites

drops from 32.81 nm to 28.1 and 25.6 nm for (0.7 and 0.9) % MFTNc samples. Because of their approximately similar ionic radii, the addition of the Fe^{3+} ion (0.63 Å) to the TiO₂ (0.68 Å) lattice causes lattice distortions by replacing Ti^{4+} and disrupting its crystal growth. Grain growth is inhibited by the oxygen vacancies and localized strain caused by this substitution. Consequently, as the Fe content rises, the crystallite size falls and the peaks shift towards lower 2θ angles as shown in the inset of Figure 1. Additionally, the absence of extra peaks in the XRD spectrum successfully confirms the Fe doping within the TiO₂ matrix. Because Fe^{3+} ions are probably incorporated into the TiO₂ lattice substitutionally at lower concentrations without forming distinct secondary phases, Fe-related peaks only show up at higher doping levels. Excess Fe exceeds the solubility limit as the doping level rises, forming distinct Fe-rich phases that can be seen using XRD. Low Fe content can also result in signals that are below the instrument's detection threshold.
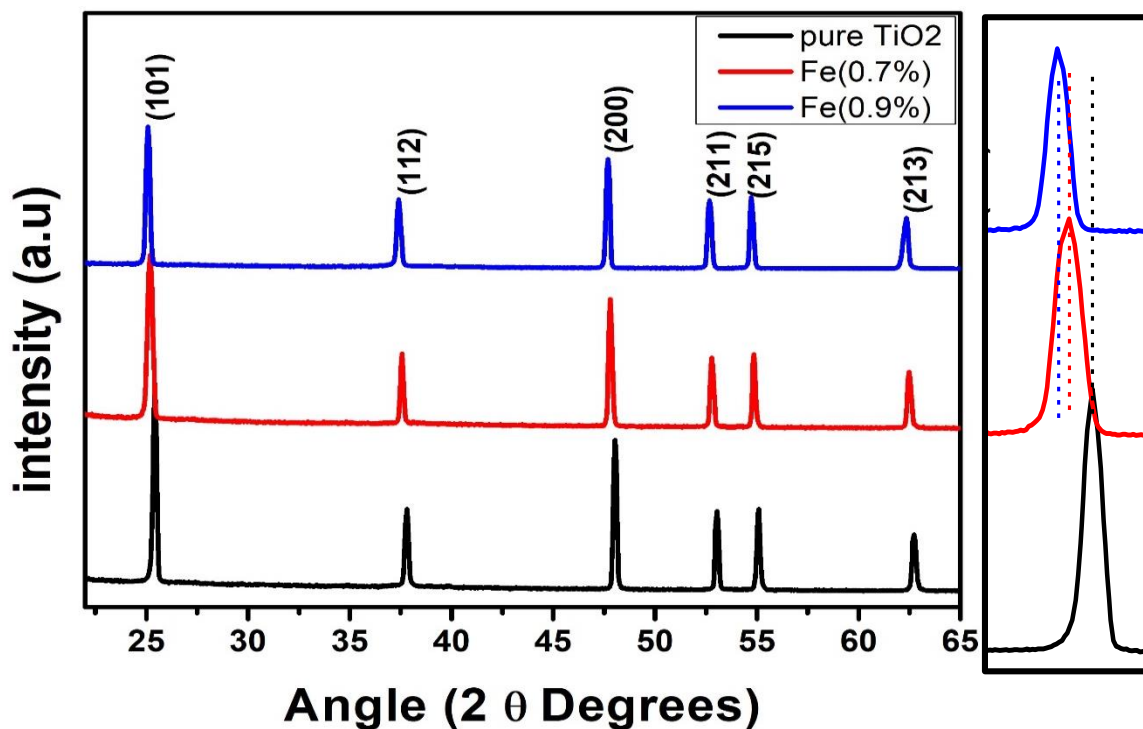

Fig. 1: Represents (XRD) trends of pure TiO₂ and all fabricated MFTNc. The diffraction peaks represent the pure anatase phase with JCPDS # 0089-4921 and show diffraction peaks corresponding to the (101), (112), (200), (211), and (215) crystallographic planes.

Table 1: Full set of physical-chemical characteristics of pure and MFTNc.

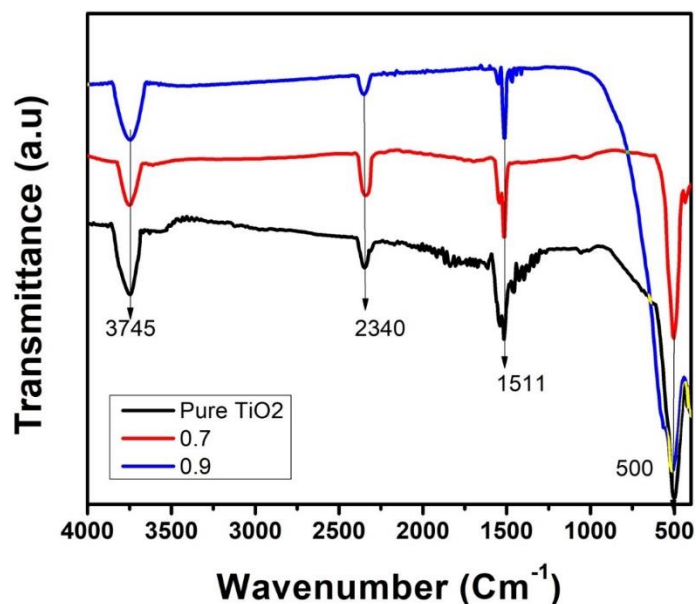| Dopant	Crystallite size	Micro strain	Dislocation Density	Crystallinity	Eg
w%	(nm)	(10^{-3})	$(nm)^{-2} \times 10^{3}$	(%)	(eV)
TiO₂-Pure	32.81	0.52	4.93	36.68	3.21
0.7% MFTNc	28.16	0.64	8.56	79.19	3.01
0.9% MFTNc	25.68	0.58	8.99	71.62	2.98

Fig. 2:   The FTIR spectra of pure TiO_2, 0.7%, and 0.9% MFTNc all display distinctive vibrational peaks. O-H stretching vibrations, which indicate surface-adsorbed water or hydroxyl groups, are represented by the broadband at about 3745 cm^{-1}. The band at 1511 cm^{-1} is linked to C=C aromatic stretching, which may be caused by phytochemical residues, whereas the peak at 2340 cm^{-1} is ascribed to CO_2 adsorption. The anatase phase of TiO_2 is confirmed by the strong band near 500 cm^{-1}, which represents Ti–O–Ti lattice vibrations. These bands are slightly shifted and sharpened by doping, indicating successful surface modification and Fe incorporation.

FTIR analysis

The sample that was prepared was examined using Fourier transform infrared (FTIR) spectroscopy [30]. The study examined the FTIR spectra of the Fe-doped photocatalyst sample concerning its wave number to determine the vibrational band present within the system [18]. More details of structural and phase changes in TiO_2 were discovered by the application of FTIR assessments. FTIR spectra of pure and various concentrations of integrated MFTNc catalysts, as shown in Fig. 2, were obtained range from 400–4000 cm^{-1} to determine the existence of necessary functional groups in the fabricated samples [35]. Wideband is observed in wavenumber extends within 3745 cm^{-1}, which is explained by the bending vibrations of the O–H and N–H interactions [40]. A primary set of spectral bands seen at 2340 cm^{-1} is attributed to CO_2 that has been airborne and adsorbed onto the particle surface [41]. Since it can obstruct active sites and prevent the adsorption of target pollutants, CO_2 adsorbed on the sample surface is typically harmful. It might not, however, have a major impact on photocatalytic performance in minimal quantities. When ambient oxygen enters the specimen during the fabrication and manufacturing of the NCs, a very sharp peak develops within 1511 cm^{-1} [42]. The symmetrical resonance of Fe–O–Fe bonds and the Ti–

O bonding excitation is represented by the absorption peak of 500 cm^{-1} for modified nanostructures. Due to modifications in the local bonding environment, Fe doping results in a shift in the Ti–O vibration band, which is indicative of lattice distortion. Given that Fe^{3+} (0.63 Å) and Ti^{4+} (0.68 Å) have similar ionic radii and can thus replace Ti^{4+} in the lattice, this shift implies substitutional doping. The vibrational frequency is modified by the changed mass and bonding strength, proving substitution. The bands are essential for increasing photocatalytic activity [2]. Overall, the FTIR results agreed very well with [43].

UV Analysis

The diffusing absorption spectrum of both pure and Fe-doped TiO_2 nanocomposites is shown in the UV graph in Fig. 3 (a). The samples' UV-Vis spectrum was obtained using a Shimadzu diffuse reflectance UV-vis spectrophotometer using an average scan rate and a 0.2 nm sample spacing [44]. It is evident from the spectra that TiO_2 absorbs more in the ultraviolet and less in the visible spectrum [36]. Fig. 3 (a) reveals that an increase in Fe-concentration in TiO_2 led to higher absorption in the visible spectrum of light [45]. Ultraviolet visible reflecting spectra have been employed in order to calculate the band-gap energy of TiO_2 and MFTNc, as

shown in Fig. 3 (b). The indirect band-gap energies were calculated through the tauc plot method and were significantly impacted by iron loading within TiO_2 [46]. For pure TiO_2, the primary band gap was determined to be 3.21 eV, corresponding to the anatase phase of TiO_2 with an indirect band gap [47]. Meanwhile, 0.9% of MFTNc reveals a significant reduction in the band gap value up to 2.98 eV [26] compared to 3.01 eV for the 0.7% MFTNc sample [48]. The decrease in the band gap may result from the interaction between the 3d orbital of Ti, which forms the conduction band of TiO_2, and the 3d orbital of Fe^{3+}. This interaction reduces the separation between the valence and conduction bands in the solid solution [48]. By introducing impurity states into the TiO_2 band gap, Fe doping reduces the effective band gap by acting as intermediate energy levels. This lowers the total band gap energy by making electron excitation simpler.
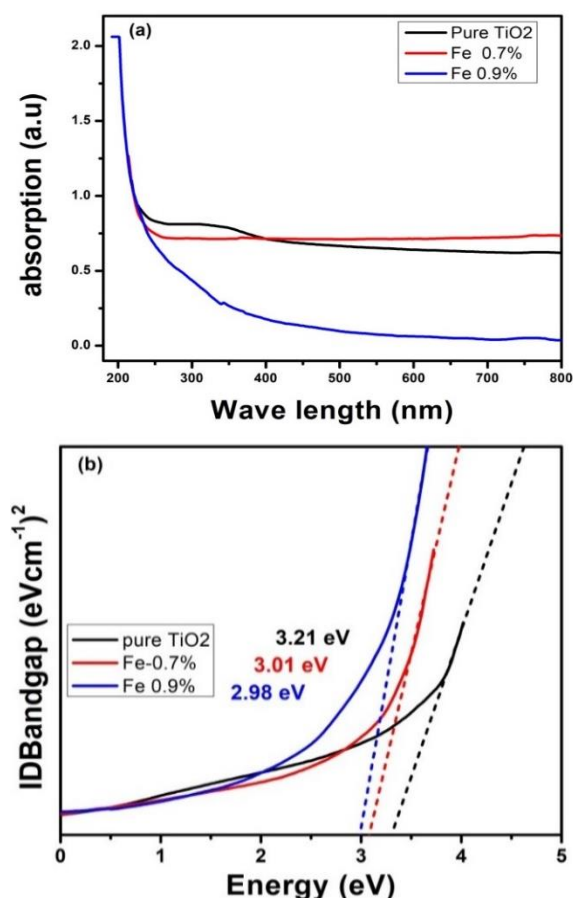

Fig. 3: (a) UV-Vis absorbance spectra and corresponding (b) Tauc plot for band gap determination of the synthesized samples of pure TiO_2 and MFTNc, showing a significant reduction in the indirect band gap value calculated through the tauc plot method.

Photocatalytic Activity of Methylene Blue (MB)

The solution was exposed to direct sunlight for 80 minutes in order to achieve the photocatalytic decomposition of MB in the presence of pure and MFTNc, as shown in Fig. 4 (a-c). Electrons migrate from the valence band (VB) to the conduction band (CB) when MFTNc is exposed to light, particularly in the visible or ultraviolet spectrum, creating holes in the VB. Light absorption creates electron-hole pairs (e^-/h^+) in the TiO_2 structure as a result of these negative charge carriers migrating toward the conduction band. These electron-hole pairs quickly recombine in undoped TiO_2, reducing photocatalytic efficiency as illustrated in Fig. 4 (a), revealing only 7.43% photodegradation of MB. Fe doping, however, enhances these charge carriers' separation; excited electrons from the CD are captured by Fe^{3+} ions. As a result, electron-hole pairs become more stable and their recombination is delayed, facilitating more effective interaction between MB molecules in the solution. Subsequently, as shown in Fig. 4(c), this enhances the photodegradation of MB by up to 35.76% when a 0.9% Ag-doped TiO_2 sample is present. Trapped electrons (e^-) can transfer to oxygen molecules in an aqueous solution, resulting in reactive oxygen species (ROS) like superoxide anions ($O_2 \bullet^-$). In the valence band, charged holes (h^+) may create hydroxyl radicals when combined with water (H_2O) or hydroxyl ions (OH^-), respectively, which are extremely reactive. ROS, specifically hydroxyl radicals and superoxide ions, are attributed to the breakdown of MB dye molecules. They target the MB dye structure, triggering the chromophore group to be cleaved and decolorized, resulting in lighter, non-toxic residues. The graph in Fig. 4 (d) shows how well pure TiO_2 and Fe-doped TiO_2 (0.7% and 0.9%, respectively) degrade MB over time. Remarkably, after 80 minutes, 0.9% Ag-doped TiO_2 maintains 35.76% degradation efficiency, demonstrating the best photodegradation performance among all the fabricated specimens. Pure TiO_2, on the other hand, exhibits only 7.43% degradation efficiency against MB. Overall, the data indicate that photocatalytic performance is enhanced with an increase in the Ag concentrations in the TiO_2 matrix up to an optimal value of 0.9%. This implies that too much Fe doping could result in the introduction of recombination centers that obstruct electron-hole separation and lower photocatalytic activity. Furthermore, the anatase phase of TiO_2 is preferred for photocatalysis because of its greater surface area, better charge carrier mobility, and lower electron-hole pair recombination rate than rutile. Stronger redox reactions are made possible by its higher conduction band position. Rutile has a lower photocatalytic efficiency, which restricts its use even though it absorbs more visible light. As a result, anatase performs better overall when it comes to breaking down pollutants when exposed to UV light.
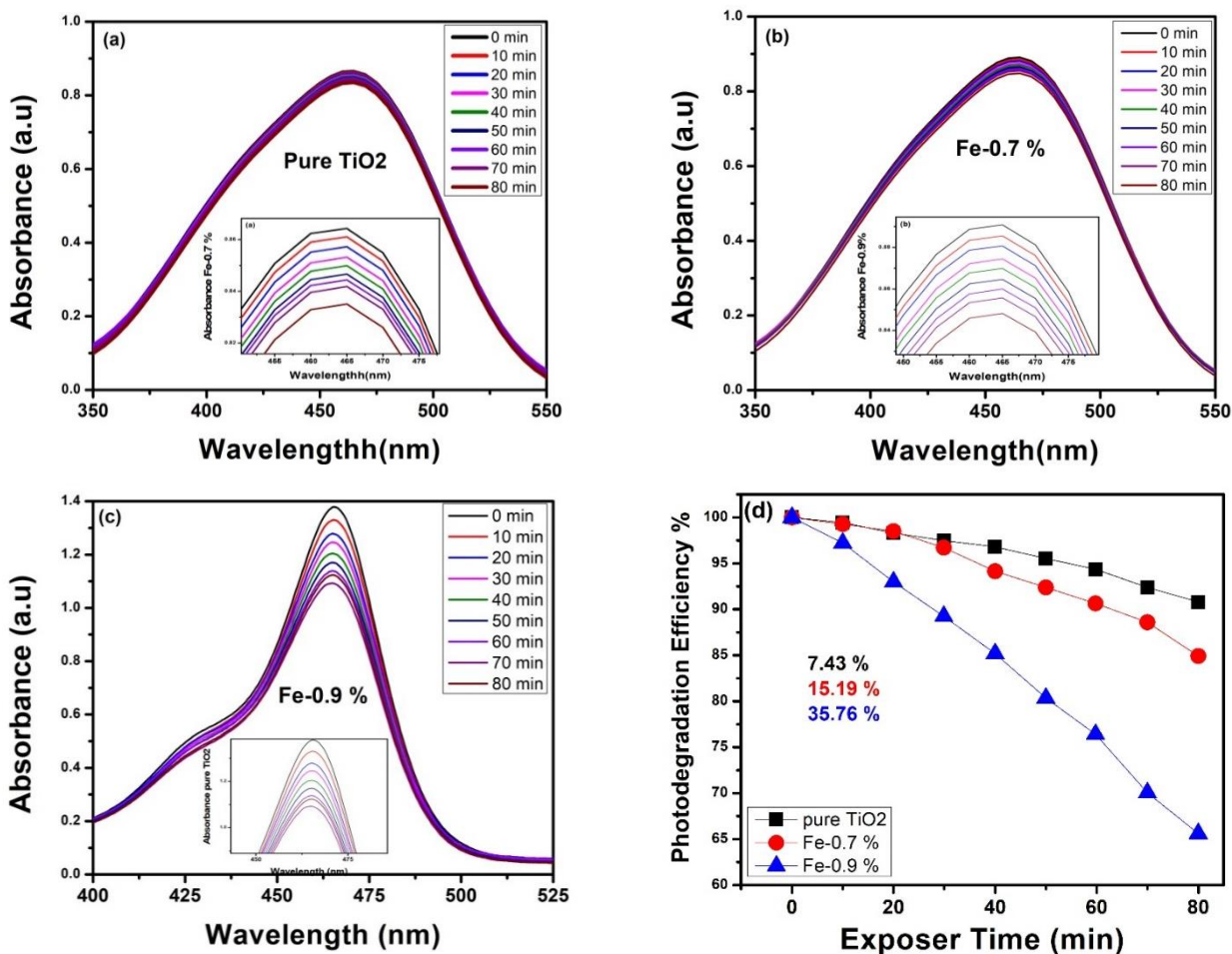
Fig. 4:   UV vis absorbance (a) Pure TiO$_2$, (b) Fe-0.7 % (c) Fe-0.9 % (d) Photodegradation Efficiency Vs Exposure Time of all the fabricated samples.

The Langmuir-Hinshelwood framework is used to demonstrate pseudo-first-order kinetics for the photodegradation of MB dye in the context of pure and MFTNc, as illustrated in Fig. 5. Because it accurately depicts surface-catalyzed reactions involving reactant adsorption on catalyst sites and fits the experimental setup, the Langmuir-Hinshelwood model was selected. It offers a realistic kinetic framework by taking into consideration both adsorption equilibrium and reaction rate. Accuracy is limited by alternatives that frequently ignore surface interactions. Consequently, it provides a well-rounded, mechanistic understanding of heterogeneous catalytic kinetics. A linear fit model was used to compute the decay rate constant, and it was shown that the degradation rate is proportional to the MB concentration.

Improvement in the decay rate constant: Fe doping results in an increase in the rate constant for

MB degradation as compared to pure TiO$_2$, indicating enhanced photocatalytic performance.

Effect of pH on the photodegradation of Methylene Blue (MB)

The pH of the reaction medium significantly influences the photocatalytic activity of Moringa extract-assisted Fe-doped TiO$_2$. Maximum photodegradation efficiency was observed at pH 6, where the surface charge of the catalyst and the ionization state of both the pollutant and phytochemicals in the extract are optimally aligned. At this near-neutral pH, electrostatic interactions between the catalyst surface and pollutant molecules are enhanced, facilitating better adsorption and charge transfer. Additionally, the stability of Fe ions and the bioactive compounds from Moringa is preserved, promoting efficient electron-hole separation and radical formation for effective degradation.
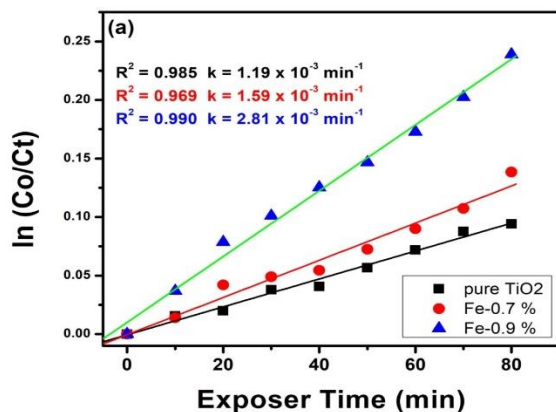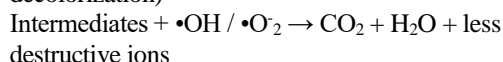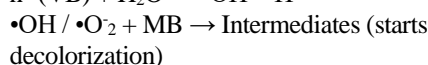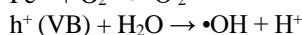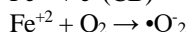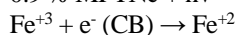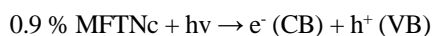
Fig. 5: Represents the pseudo-first-order kinetics model applied to the photodegradation of methylene blue (MB), comparing the degradation performance of pure TiO_2 and (MFTNc).

Photodegradation Mechanism

Apart from the degradation initiated by ROS, MB molecules can also be directly oxidized by the photo-created holes (h^+) in the valence band; this direct oxidation path further aids in the photodegradation of MB. Hydroxyl radical harassment, superoxide radical operations, and direct hole oxidation work together to convert MB into less complex molecules like water (H_2O), carbon dioxide (CO_2), and other innocuous byproducts. To maximize photocatalytic performance, the concentration of the Fe-dopant played an essential role during the breakdown of MB. While visible light absorption and charge separation are improved by an ideal Fe dopant concentration [49]. In our case, we observed that the 0.9% MFTNc sample shows maximum photodegradation efficiency of MB 22.5 % as compared to 16 & 9.25 % for 0.3 % Fe-doped and pure TiO_2, respectively.

$0.9 \% \text{ MFTNc} + h\nu \rightarrow e^- (CB) + h^+ (VB)$
$Fe^{+3} + e^- (CB) \rightarrow Fe^{+2}$
$Fe^{+2} + O_2 \rightarrow \bullet O_2^-$
$h^+ (VB) + H_2O \rightarrow \bullet OH + H^+$
$\bullet OH / \bullet O_2^- + MB \rightarrow \text{Intermediates (starts decolorization)}$
$\text{Intermediates} + \bullet OH / \bullet O_2^- \rightarrow CO_2 + H_2O + \text{less destructive ions}$

Incorporating Fe^{+3} ions into the TiO_2 crystal lattice accelerates methylene blue disintegration overall due to enhanced separation of charge carriers and increased absorption of light in the visible spectrum. The photodegradation mechanism of MB in the presence of the MFTNc is illustrated in Fig. 6.
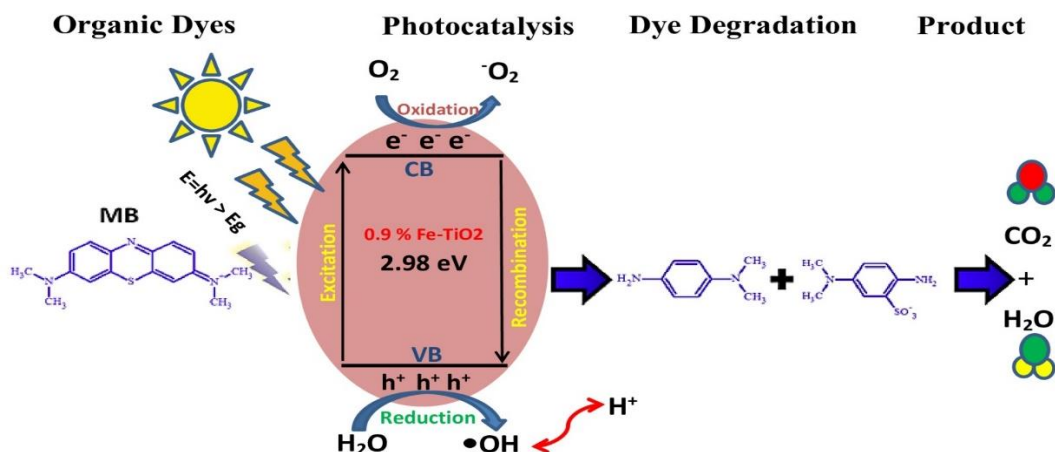

Fig. 6: Schematic representation of the photodegradation mechanism of methylene blue (MB) under visible light irradiation in the presence of pure TiO_2 and MFTNc. Diagrammatic illustration of the process by which 0.9% Fe-doped TiO_2 breaks down methylene blue (MB) dye when exposed to light. When exposed to photons with energy higher than the bandgap (2.98 eV), electrons (e^-) are excited from the valence band (VB) to the conduction band (CB), producing electron-hole (e^-/h^+) pairs. Superoxide radicals ($\bullet O_2^-$) are created when photogenerated electrons reduce molecular oxygen (O_2), and hydroxyl radicals ($\bullet OH$) are created when holes oxidize water molecules. The dye molecules are actively broken down by these reactive oxygen species (ROS) into intermediate aromatic compounds, which are then mineralized into innocuous byproducts like CO_2 and H_2O. Excessive Fe doping, however, could result in more charge recombination and lower total photocatalytic efficiency.

Table 2: Comparison of current research with previous similar studies

Photocatalyst	Dye	Quantity	Light Source	Degradation%	Time	Ref
TiO_2-0.32Fe	MB	15 mg/L	Xe-lamp 90W	24.4	90 min	[50]
ZnO	MB	20 mg/L	-----------	28.75	60 min	[51]
ZnO	MB	20 mg/dm^3	Sunlight	3.8	90min	[52]
ZFO-SnO_2	MB	1 g/L	Xe-lamp	10.1	60 min	[53]
g-C_3N_4	MB	10ppm	LED-20W	22.60	150min	[54]
C-CeO_2	MB	12.5-mg/L	------------	17	210 min	[55]
0.9 % MFTNc	MB	10 mg/L	Sunlight	35.76	80 min	Current work

Table II provides a comparison between the current study and similar research efforts reported in the literature. The results of this study demonstrate superior performance compared to several previous works.

Conclusion

Using Moringa plant extract as a natural stabilizer and reducing agent, this work represents the first successful synthesis of Fe-doped TiO_2 nanocomposites (MFTNc) using a green, two-step sol-gel method. Crystallite size dropped from about 32.8 nm (pure TiO_2) to about 28.1 nm (0.7%) and about 25.6 nm for (0.7 & 0.9) % Fe-doped TiO_2 nanocrystals without the formation of undesired phases, according to structural analyses XRD, FTIR, and UV-vis spectroscopy that verified Fe^{3+} ions integrate into the anatase TiO_2 lattice, causing controlled lattice distortion and size reduction. The band gap gradually redshifted from 3.21 eV (pure TiO_2) to 3.01 eV and 2.98 eV for 0.7% and 0.9% Fe-doped TiO_2 samples, respectively, according to optical characterization, allowing for visible-light absorption. Methylene blue photocatalytic tests conducted in natural sunlight showed a notable improvement in degradation efficiency, with 0.9% MFTNc samples achieving 35.8% degradation in 80 minutes as opposed to only 7.4% for pure TiO_2. The extremely minimal solar irradiance (1.5 W $m^{-2} s^{-1}$), which restricts the generation of electron-hole pairs, is the principal cause of the comparatively restricted photocatalytic efficiency (35.76%) pursuant to optimal Fe doping (0.9%). Fe^{3+} cycling is thought to be the mechanism, acting as electron traps, lowering electron-hole recombination, and promoting the production of reactive oxygen species (ROS). Ideal surface charge interactions and strong stability of both Fe and phytochemicals were responsible for the optimal photocatalytic activity that was seen close to neutral pH-6. Future research should assess the long-term stability and recyclability of photocatalysts, optimize the concentration of iron, and investigate alternative pollutant systems.

Acknowledgment

Conflict of Interest:

The authors declare that there are no conflicts of interest regarding the publication of this work.

References

1. H. Mohammad-Salehi, M. Hamadanian, and H. Safardoust-Hojaghan, "Visible-Light Induced Photodegradation of Methyl Orange via Palladium Nanoparticles Anchored to Chrome and Nitrogen Doped TiO2 Nanoparticles," *J. Inorg. Organomet. Polym. Mater.*, vol. 29, no. 5, pp. 1457–1465, 2019, doi: 10.1007/s10904-019-01109-z.

2. K. I. Dhanalekshmi, P. Magesan, M. J. Umapathy, X. Zhang, N. Srinivasan, and K. Jayamoorthy, "Enhanced photocatalytic and photodynamic activity of chitosan and garlic loaded CdO–TiO2 hybrid bionanomaterials," *Sci. Rep.*, vol. 11, no. 1, p. 20790, Oct. 2021, doi: 10.1038/s41598-021-00242-5.

3. S. F. Lee, E. Jimenez-Relinque, I. Martinez, and M. Castellote, "Effects of Mott–Schottky Frequency Selection and Other Controlling Factors on Flat-Band Potential and Band-Edge Position Determination of TiO2," *Catalysts*, vol. 13, no. 6, p. 1000, Jun. 2023, doi: 10.3390/catal13061000.

4. N. Xie, T. J. DiChristina, and M. Taillefert, "Impact of orthophosphate on the light-independent production of reactive oxygen species during microbially-mediated Fe redox cycles," *Appl. Geochemistry*, vol. 156, p. 105739, Sep. 2023, doi: 10.1016/j.apgeochem.2023.105739.

5. T. Wu, Y. Liu, T. Zheng, Y. Dai, Z. Li, and D. Lin, "Fe-Based Nanomaterials and Plant Growth Promoting Rhizobacteria Synergistically Degrade Polychlorinated Biphenyls by Producing Extracellular Reactive Oxygen Species," *Environ. Sci. Technol.*, vol. 57, no. 34, pp. 12771–12781,

Aug. 2023, doi: 10.1021/acs.est.3c02495.

6. G. Foura, N. Chouchou, K. Kouachi, and M. Guidotti, "Fe-Doped TiO 2 Supported on HY Zeolite for Solar," vol. 2, no. i, 2017, doi: 10.3390/catal7110344.

7. K. H. Lee *et al.*, "The Comparison of Metal Doped TiO2 Photocatalytic Active Fabrics under Sunlight for Waste Water Treatment Applications," *Catalysts*, vol. 13, no. 9, 2023, doi: 10.3390/catal13091293.

8. S. Madhav, A. Ahamad, P. Singh, and P. K. Mishra, "A review of textile industry: Wet processing, environmental impacts, and effluent treatment methods," *Environ. Qual. Manag.*, vol. 27, no. 3, pp. 31–41, Mar. 2018, doi: 10.1002/tqem.21538.

9. S. Malik, K. Muhammad, and Y. Waheed, "Nanotechnology: A Revolution in Modern Industry," *Molecules*, vol. 28, no. 2, p. 661, Jan. 2023, doi: 10.3390/molecules28020661.

10. M. A. Ahmed, E. E. El-katori, and Z. H. Gharni, "Photocatalytic degradation of methylene blue dye using Fe 2 O 3 / TiO 2 nanoparticles prepared by sol – gel method," *J. Alloys Compd.*, vol. 553, pp. 19–29, 2013, doi: 10.1016/j.jallcom.2012.10.038.

11. Q. I. Rahman, M. Ahmad, S. K. Misra, and M. Lohani, "Effective photocatalytic degradation of rhodamine B dye by ZnO nanoparticles," *Mater. Lett.*, vol. 91, pp. 170–174, 2013, doi: 10.1016/j.matlet.2012.09.044.

12. S. Ahadi, N. S. Moalej, and S. Sheibani, "Characteristics and photocatalytic behavior of Fe and Cu doped TiO 2 prepared by combined sol-gel and mechanical alloying," *Solid State Sci.*, vol. 96, no. May, p. 105975, 2019, doi: 10.1016/j.solidstatesciences.2019.105975.

13. M. Gharagozlou and S. Zhahabi, "Synthesis and Characterization of Novel Hybrid Nanocomposite containing Modified Titanium Dioxide Nanoparticles with Copper and Phthalocyanine Pigment," *Nanochemistry Res.*, vol. 6, no. 1, pp. 94–103, 2021, doi: 10.22036/NCR.2021.01.009.

14. S. Munir, F. Asghar, F. Younis, S. Tabassum, A. Shah, and S. B. Khan, "Assessing the potential biological activities of TiO2and Cu, Ni and Cr doped TiO2nanoparticles," *RSC Adv.*, vol. 12, no. 7, pp. 3856–3861, 2022, doi: 10.1039/d1ra07336b.

15. S. Al Jitan, G. Palmisano, and C. Garlisi, "Synthesis and Surface Modification of TiO2-Based Photocatalysts for the Conversion of CO2," *Catalysts*, vol. 10, no. 2, p. 227, Feb. 2020, doi: 10.3390/catal10020227.

16. A. Eshaghi and H. Moradi, "Optical and photocatalytic properties of the Fe-doped TiO 2 nanoparticles loaded on the activated carbon," *Adv. Powder Technol.*, no. May, 2018, doi: 10.1016/j.apt.2018.04.026.

17. A. M. Wu, P. Wu, T. Lin, and T. Lin, "Photocatalytic Performance of Cu-doped TiO 2 Nanofibers Treated by," *Appl. Surf. Sci.*, 2017, doi: 10.1016/j.apsusc.2017.09.035.

18. T. Ali *et al.*, "Photocatalytic performance of Fe-doped TiO 2 nanoparticles under visible-light irradiation," *Mater. Res. Express*, vol. 4, no. 1, p. 015022, Jan. 2017, doi: 10.1088/2053-1591/aa576d.

19. C. Karunakaran, G. Abiramasundari, P. Gomathisankar, G. Manikandan, and V. Anandi, "Journal of Colloid and Interface Science Cu-doped TiO 2 nanoparticles for photocatalytic disinfection of bacteria under visible light," *J. Colloid Interface Sci.*, vol. 352, no. 1, pp. 68–74, 2010, doi: 10.1016/j.jcis.2010.08.012.

20. S. M. Reda, M. A. Khairy, and M. A. Mousa, "Photocatalytic Activity of Nitrogen and Copper Doped TiO 2 Nanoparticles Prepared by Microwave-Assisted Sol-Gel Process," *Arab. J. Chem.*, 2017, doi: 10.1016/j.arabjc.2017.02.002.

21. T. Perarasan, I. J. Peter, A. M. Kumar, N. Rajamanickam, K. Ramachandran, and C. R. Mohan, "Copper doped titanium dioxide for enhancing the photovoltaic behavior in solar cell," *Mater. Today Proc.*, vol. 35, no. 3, pp. 66–68, 2019, doi: 10.1016/j.matpr.2019.06.377.

22. M. Maicu, M. C. Hidalgo, and J. A. Navı, "Cu-doped TiO 2 systems with improved photocatalytic activity," vol. 67, pp. 41–51, 2006, doi: 10.1016/j.apcatb.2006.03.019.

23. V. Thongpool, A. Phunpueok, S. Jaiyen, and T. Sornkwan, "Results in Physics Synthesis and photocatalytic activity of copper and nitrogen co-doped titanium dioxide nanoparticles," *Results Phys.*, vol. 16, no. January, p. 102948, 2020, doi: 10.1016/j.rinp.2020.102948.

24. F. Tio, A. Mancuso, O. Sacco, D. Sannino, S. Pragliola, and V. Vaiano, "Enhanced visible-light-driven photodegradation of Acid Orange 7 azo dye in aqueous solution using," *Arab. J. Chem.*, 2020, doi: 10.1016/j.arabjc.2020.05.019.

25. A. El Mragui, Y. Logvina, O. Zegaoui, and J. C. G. Esteves, "Photocatalytic Activity Under Visible Irradiation Toward Carbamazepine Degradation," pp. 4–6, 2019.

26. T. T. Loan, V. H. Huong, N. T. Huyen, L. Van Quyet, N. A. Bang, and N. N. Long, "Anatase to rutile phase transformation of iron-doped titanium dioxide nanoparticles: The role of iron content," *Opt. Mater. (Amst).*, vol. 111, no. November, p. 110651, 2021, doi: 10.1016/j.optmat.2020.110651.

27. A. Garg *et al.*, "Photocatalytic Degradation of Bisphenol-A using N, Co Codoped TiO2 Catalyst under Solar Light," *Sci. Rep.*, vol. 9, no. 1, pp. 1–13, 2019, doi: 10.1038/s41598-018-38358-w.

28. M. H. Dehghani, S. Afsari Sardari, M. Afsharnia, M. Qasemi, and M. Shams, "Removal of toxic lead from aqueous solution using a low-cost adsorbent," *Sci. Rep.*, vol. 13, no. 1, p. 3278, Feb. 2023, doi: 10.1038/s41598-023-29674-x.

29. M. Manzoor, A. Rafiq, M. Ikram, M. Nafees, and S. Ali, "Structural, optical, and magnetic study of Ni-doped TiO2 nanoparticles synthesized by sol–gel method," *Int. Nano Lett.*, vol. 8, no. 1, pp. 1–8, 2018, doi: 10.1007/s40089-018-0225-7.

30. L. J. K. and Y. Syahputri, "Study of structural and optical properties of Fe (III) -doped TiO 2 prepared by sol-gel method Study of structural and optical properties of Fe (III) -doped TiO prepared by sol-gel method," no. Iii, 2019, doi: 10.1088/1755-1315/299/1/012066.

31. T. Barkhade, I. Banerjee, T. Barkhade, and I. Banerjee, "Photocatalytic Degradation of Rhodamine B Dye Using Fe doped TiO 2 Nanocomposites," vol. 030016, 2018, doi: 10.1063/1.5035218.

32. N. Cai, Y. Mai, R. Su, and D. Lv, "Synthesis of porous TiO2 and Fe-doped TiO2 films for photocatalysis by a cooling enhanced plasma electrolytic oxidation approach," *Mater. Lett.*, vol. 365, p. 136464, Jun. 2024, doi: 10.1016/j.matlet.2024.136464.

33. V. Uthiravel, K. Narayanamurthi, V. Raja, S. Anandhabasker, and K. Kuppusamy, "Green synthesis and characterization of TiO2 and Ag-doped TiO2 nanoparticles for photocatalytic and antimicrobial applications," *Inorg. Chem. Commun.*, vol. 170, p. 113327, Dec. 2024, doi: 10.1016/j.inoche.2024.113327.

34. Swati *et al.*, "Antimicrobial potential of ag-doped ZnO nanostructure synthesized by the green method using moringa oleifera extract," *J. Environ. Chem. Eng.*, vol. 8, no. 3, p. 103730, Jun. 2020, doi: 10.1016/j.jece.2020.103730.

35. C. R. S. K. Amarsingh and B. T. R. Rajasekaran, "Enhanced electrochemical behavior of novel acceptor doped titanium dioxide catalysts for photocatalytic applications," *J. Mater. Sci. Mater. Electron.*, vol. 0, no. 0, p. 0, 2017, doi: 10.1007/s10854-017-6396-6.

36. D. Komaraiah, E. Radha, N. Kalarikkal, J. Sivakumar, M. V. R. Reddy, and R. Sayanna, "Structural , optical and photoluminescence studies of sol-gel synthesized pure and iron doped TiO 2 photocatalysts," *Ceram. Int.*, vol. 45, no. 18, pp. 25060–25068, 2019, doi: 10.1016/j.ceramint.2019.03.170.

37. H. Moradi, A. Eshaghi, S. R. Hosseini, and K. Ghani, "Fabrication of Fe-doped TiO2 nanoparticles and investigation of photocatalytic decolorization of reactive red 198 under visible light irradiation," *Ultrason. Sonochem.*, 2016, doi: 10.1016/j.ultsonch.2016.03.025.

38. X. Zheng, J. Zhang, X. Yang, and W. Cao, "Journal of Physics and Chemistry of Solids Synthesis and application of the solar cell of poly (3-hexylthiophene)/ Fe N / titanium dioxide nanocomposite material," *J. Phys. Chem. Solids*, vol. 72, no. 3, pp. 220–226, 2011, doi: 10.1016/j.jpcs.2010.12.015.

39. S. Saroj, L. Singh, R. Ranjan, and S. V. Singh, "Enhancement of photocatalytic activity and regeneration of Fe-doped -TiO 2 -(Ti 1−," no. 0123456789, 2019, doi: 10.1007/s11164-018-3708-2.

40. J. Yu, H. Yu, C. H. Ao, S. C. Lee, J. C. Yu, and W. Ho, "Preparation , characterization and photocatalytic activity of in situ Fe-doped TiO 2 thin films," vol. 496, pp. 273–280, 2006, doi: 10.1016/j.tsf.2005.08.352.

41. J. Wang *et al.*, "The effects of additive on properties of Fe doped TiO 2 nanoparticles by modi fi ed sol-gel method," no. xxxx, 2020, doi: 10.1016/j.jallcom.2020.157726.

42. B. Khoshnevisan, M. B. Marami, and M. Farahmandjou, "Fe3+-Doped Anatase TiO2 Study Prepared by New Sol-Gel Precursors," *Chinese Phys. Lett.*, vol. 35, no. 2, 2018, doi: 10.1088/0256-307X/35/2/027501.

43. C. L. Luu, Q. T. Nguyen, and S. T. Ho, "Synthesis and characterization of Fe-doped TiO 2 photocatalyst by the sol–gel method," *Adv. Nat. Sci. Nanosci. Nanotechnol.*, vol. 1, no. 1, p. 015008, Mar. 2010, doi: 10.1088/2043-6254/1/1/015008.

44. F. A. Unal, S. Ok, M. Unal, S. Topal, K. Cellat, and F. Şen, "Synthesis, characterization, and application of transition metals (Ni, Zr, and Fe) doped TiO2 photoelectrodes for dye-sensitized solar cells," *J. Mol. Liq.*, vol. 299, p. 112177, 2020, doi: 10.1016/j.molliq.2019.112177.

45. I. Ganesh *et al.*, "Preparation and characterization of Co-doped TiO 2 materials for solar light induced current and photocatalytic applications," *Mater. Chem. Phys.*, vol. 135, no. 1, pp. 220–234, 2012, doi: 10.1016/j.matchemphys.2012.04.062.

46. A. Zuorro, R. Lavecchia, M. M. Monaco, G. Iervolino, and V. Vaiano, "Photocatalytic degradation of azo dye reactive violet 5 on fe-doped titania catalysts under visible light irradiation," *Catalysts*, vol. 9, no. 8, 2019, doi: 10.3390/catal9080645.

47. M. Jahdi, S. B. Mishra, E. N. Nxumalo, S. D.

Mhlanga, and A. K. Mishra, "Synergistic effects of sodium fluoride (NaF) on the crystallinity and band gap of Fe-doped TiO2 developed via microwave-assisted hydrothermal treatment," *Opt. Mater. (Amst).*, vol. 104, no. October 2019, p. 109844, 2020, doi: 10.1016/j.optmat.2020.109844.

48. N. R. Mathews, M. A. C. Jacome, E. R. Morales, and J. A. T. Antonio, "Structural and spectroscopic study of the Fe doped TiO2 thin films for applications in photocatalysis," *Phys. Status Solidi Curr. Top. Solid State Phys.*, vol. 6, no. SUPPL. 1, pp. 219–223, 2009, doi: 10.1002/pssc.200881319.

49. S. Sood, A. Umar, S. K. Mehta, and S. K. Kansal, "Highly effective Fe-doped TiO2 nanoparticles photocatalysts for visible-light driven photocatalytic degradation of toxic organic compounds," *J. Colloid Interface Sci.*, vol. 450, pp. 213–223, 2015, doi: 10.1016/j.jcis.2015.03.018.

50. S. Larumbe, M. Monge, and C. Gómez-Polo, "Comparative study of (N, Fe) doped TiO 2 photocatalysts," *Appl. Surf. Sci.*, vol. 327, pp. 490–497, 2015, doi: 10.1016/j.apsusc.2014.11.137.

51. J. Lin, Z. Luo, J. Liu, and P. Li, "Photocatalytic degradation of methylene blue in aqueous solution by using ZnO-SnO2 nanocomposites," *Mater. Sci. Semicond. Process.*, vol. 87, no. 20, pp. 24–31, 2018, doi: 10.1016/j.mssp.2018.07.003.

52. O. Długosz and M. Banach, "ZnO–SnO2–Sn nanocomposite as photocatalyst in ultraviolet and visible light," *Appl. Nanosci.*, vol. 11, no. 5, pp. 1707–1719, May 2021, doi: 10.1007/s13204-021-01788-6.

53. L. Guo, N. Okinaka, L. Zhang, and S. Watanabe, "Facile synthesis of ZnFe2O4/SnO2 composites for efficient photocatalytic degradation of methylene blue," *Mater. Chem. Phys.*, vol. 262, p. 124273, 2021, doi: 10.1016/j.matchemphys.2021.124273.

54. P. L. Yee, L. C. Sim, S. H. Shuit, K. H. Leong, and Y. H. Chin, "Oxygen Functionalized Graphitic Carbon Nitride for Photocatalytic Degradation of Dye," *IOP Conf. Ser. Earth Environ. Sci.*, vol. 1303, no. 1, 2024, doi: 10.1088/1755-1315/1303/1/012018.

55. S. Sehar *et al.*, "Shape-controlled synthesis of cerium oxide nanoparticles for efficient dye photodegradation and antibacterial activities," *Appl. Organomet. Chem.*, vol. 35, no. 1, pp. 1–10, 2021, doi: 10.1002/aoc.6069.